Journal of Advanced Ceramics
2019, **8**(4): 519–526
https://doi.org/10.1007/s40145-019-0333-5
ISSN 2226-4108
CN 10-1154/TQ

Research Article

Ba substitution for enhancement of the thermoelectric properties of $LaCoO_3$ ceramics ($0 \leqslant x \leqslant 0.75$)

Mohamed Ali BOUSNINA[a,b], Fabien GIOVANNELLI[a], Loïc PERRIERE[c], Guillaume GUEGAN[d], Fabian DELORME[a,*]

[a]*Université François Rabelais de Tours, CNRS, INSA CVL, GREMAN UMR7347, IUT de Blois, 15 rue de la chocolaterie, CS2903, F-41029 Blois Cedex, France*
[b]*Université Paris 13, Sorbonne Paris Cite, Laboratoire des Sciences des Procédés et des Matériaux, CNRS, UPR 3407, 99 avenue J.B. Clément, F-93430 Villetaneuse, France*
[c]*Institut de Chimie et des Matériaux Paris-Est, UMR 7182 CNRS-UPEC, 2-8 Rue Henri Dunant, 94320 Thiais, France*
[d]*ST Microelectronics, 16 Rue Pierre et Marie Curie, Tours 37100, France*

Received: March 16, 2019; Revised: April 10, 2019; Accepted: April 15, 2019

Abstract: In the present work, dense perovskite ceramics were successfully prepared from a series of $La_{1-x}Ba_xCoO_3$ solid solutions in the range of substitution $0 \leqslant x \leqslant 0.75$ using solid state reaction and conventional sintering. Structural properties of $La_{1-x}Ba_xCoO_3$ were systematically investigated and thermoelectric properties were measured in the temperature range of 330–1000 K. The results show that the thermoelectric properties of Ba-substituted $LaCoO_3$ depend on x. Indeed, at 330 K, electrical conductivity presents an optimum value for $x = 0.25$ with a value of $\sigma_{max} \approx 2.2\times10^5$ S·m^{-1} whereas the Seebeck coefficient decreases when x and/or the temperature increases. The Ba-substituted $LaCoO_3$ samples exhibit p-type semiconducting behaviour. The best power factor value found is 3.4×10^{-4} W·m^{-1}·K^{-2} at 330 K for $x = 0.075$, which is 10% higher than the optimum value measured in $La_{1-x}Sr_xCoO_3$ for $x = 0.05$. The thermal diffusivity and thermal conductivity increase with increasing temperature and Ba concentration. $La_{1-x}Ba_xCoO_3$ shows a maximum figure of merit (ZT = 0.048) for $x = 0.05$ at 330 K, 25% higher than the best value in $La_{1-x}Sr_xCoO_3$ compounds.

Keywords: perovskite; Ba-substituted $LaCoO_3$; oxide; thermoelectric; p-type semiconductor

1 Introduction

The efficiency of a thermoelectric material η depends on the thermoelectric figure of merit $ZT = S^2\sigma T/\kappa = PF\cdot T/\kappa$, where T is the absolute temperature, S is the Seebeck coefficient, σ is the electrical conductivity, κ is the thermal conductivity, and PF is the power factor. Therefore and in general, efficient thermoelectric material exhibits large absolute S, high electrical conductivity (leading to a high PF), and low thermal conductivity.

Perovskite-like lanthanum cobalt oxides $LaCoO_3$ attract much interest since the 1950s with many controversial explanations of their peculiar structural [1,2] and physical properties [3–5]. The physical properties found in these materials are varied, including

* Corresponding author.
E-mail: fabiandelorme@yahoo.fr

the change in the spin states of cobalt ions, insulator–metal phase transitions as well as various types of orbital, charge, and electric ordering. In this regard, cobalt perovskite oxides are considered as promising thermoelectric materials since the discovery of large S and PF in the metallic oxide Na_xCoO_2 in 1997 [6] as many other cobalt oxides such as $Ca_3Co_4O_9$ [7–11], $[Sr_2O_2]_qCoO_2$ [12], $Bi_2Sr_2Co_2O_y$-like [13–15], and more recently $Ba_2Co_9O_{14}$ [16,17] or Na-doped CoO [18].

Indeed, on the contrary to all the other cobalt oxides that present high thermoelectric properties at high temperatures, Androulakis *et al*. [19] have reported in $La_{1-x}Sr_xCoO_3$ (x = 0.05), the highest thermoelectric properties for an oxide at 300 K (ZT = 0.18). Therefore, Sr substituted $LaCoO_3$ ceramics have been largely studied [20–23] and the optimum value for thermoelectric properties is obtained for x = 0.05. Moreover, Bousnina *et al*. [23] have shown that the substitution can be realized up to x = 0.8 without any addition and up to x = 1 for an additional substitution of 3% Si for Co.

Calcium and barium substitutions for lanthanum have probably been less studied than the strontium for lanthanum substitution [24–26]. However, in the case of the Ba-substituted $LaCoO_3$, different magnetic and electrical behaviours have been reported for different degrees of substitution [27–29]. Indeed, substitution of La^{3+} with Ba^{2+} leads in enhanced oxide ion conductivity in the samples up to certain Ba content [30]. Furthermore, this substitution improves electrical conductivity of $La_{1-x}Ba_xCoO_3$ as for Sr-substituted samples. Moreover, as barium is heavier than strontium, a lower thermal conductivity is expected.

Therefore, the aim of this work is to synthesize, sinter, and characterize the thermoelectric properties of dense $La_{1-x}Ba_xCoO_3$ ceramics.

2 Materials and methods

La_2O_3 (Sigma Aldrich, purity $\geqslant$ 99%), Co_3O_4 (Sigma Aldrich, no specified purity), and $BaCO_3$ (Sigma Aldrich, purity $\geqslant$ 99%) were used to synthesize $La_{1-x}Ba_xCoO_3$ ($0 \leqslant x \leqslant 0.75$) by conventional solid state reaction. The precursor La_2O_3 was preheated at 1073 K for 2 h to remove any trace of lanthanum hydroxide ($La(OH_3)$) which may be originated to air hydration. Stoichiometric amounts of the precursors were well mixed for 5 min at 400 rpm in an agate ball mill (Retsch PM 100). The powders were pelletized with a small amount of PVA (5% weight) as binder. To avoid any contamination, the pellets were placed on $LaCoO_3$ previously sintered pellets deposited on zirconia beads in an alumina crucible. They were calcined at 1273 K for 12 h in air with a heating rate of 5 $K \cdot min^{-1}$, and slowly cooled down. This step has been repeated twice after manual grinding. Finally, the calcined samples were pressed into pellets, and sintered for 12 h in air at 1673 K [23].

X-ray diffraction (XRD) was performed at room temperature, on the pellets after sintering, using BRUKER D8 Advance $\theta/2\theta$ diffractometer equipped with a Linxeye energy-dispersive one-dimensional detector. The data have been recorded, using Cu Kα radiation, from 5° to 85° (2θ) with a step of 0.02° and a counting time of 2 s per step. Rietveld refinement was carried out using Fullprof software [31] to determine the samples lattice parameters.

Microstructure was examined using Zeiss Supra 40 VP Field Emission Gun Scanning Electron Microscope (FEG-SEM) without prior coating of the samples.

Thermoelectric properties of the sintered samples were determined from simultaneous measurement of Seebeck coefficient and electrical conductivity in ZEM-3 equipment (ULVAC Technologies) from 323 to 1000 K. The thermal diffusivity was measured three times using the laser flash technique (Netzsch LFA 457) from 298 to 1000 K in air. The heat capacity of the materials was measured from 298 to 1073 K, using differential scanning calorimetry (Netzsch Pegasus 404 F1), with a heating rate of 20 $K \cdot min^{-1}$ in platinum crucibles with alumina liners in argon atmosphere.

Apparent density of the samples was calculated from the weight and dimensions of the bars cut apparent density from the pellets for ZEM-3 characterization and the theoretical value [32].

3 Results and discussion

The XRD patterns in Fig. 1 can be assigned to the perovskite structure. Pure phase has been obtained without the appearance of impurities over the whole composition range of the solid solution ($0 \leqslant x \leqslant 0.75$). For higher Ba contents, samples do not present a cubic perovskite structure anymore. On the contrary to Sr-substituted samples, a 3% substitution of silicon for cobalt does not allow to stabilize the cubic perovskite structure. The XRD patterns of samples after sintering

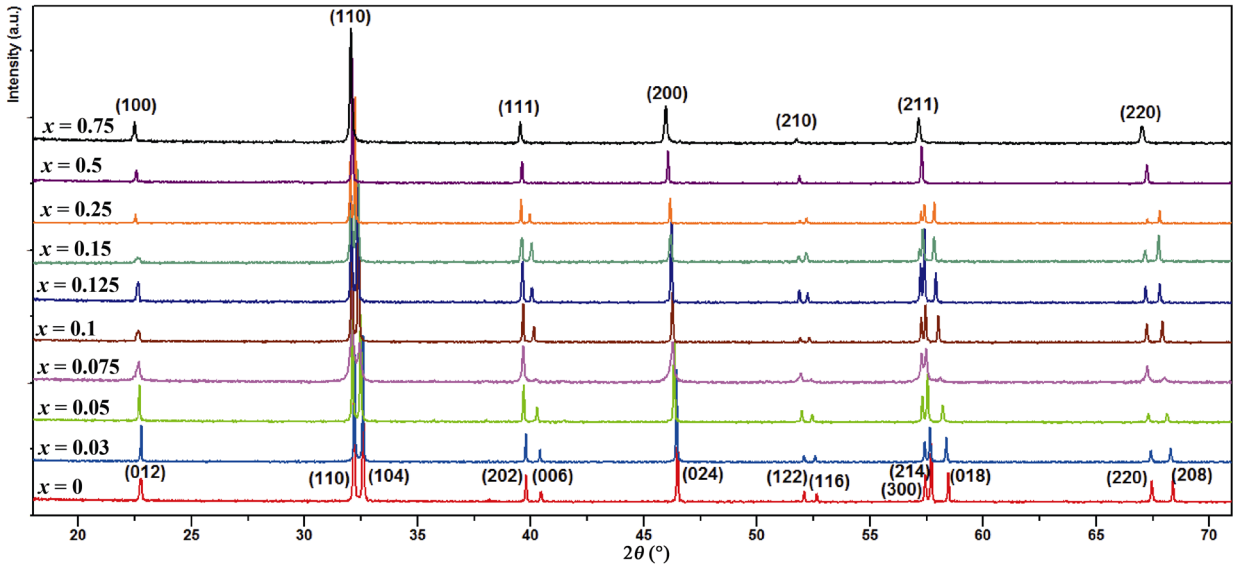

Fig. 1 XRD patterns of the $La_{1-x}Ba_xCoO_3$ solid solution at room temperature with $0 \leqslant x \leqslant 0.75$.

were analyzed by Rietveld refinement using Fullprof software [31]. The results of the refined structural parameters show a phase transition depending on the Ba concentration. XRD patterns show a gradual transition from rhombohedral to cubic perovskite phase (Fig. 1). For the low values of x, this phase transition is mainly manifested by the doubling of the diffraction peaks located at 32°, 40°, 52°, and 68° of 2θ. It is clear that the diffraction double peaks reduce to single peaks with increasing barium content, which indicates that a structure phase transition has occurred. Figure 2 presents the examples of a Fullprof software fit of the XRD pattern for representative samples of the two phases, rhombohedral and cubic perovskite. For $0 \leqslant x < 0.5$, the refinement result confirms the rhombohedral perovskite structure type of the $LaCoO_3$ ($R\bar{3}c$ space group, PDF Card No. 48-0123 [32]). The $La_{0.9}Ba_{0.1}CoO_3$ sample is displayed in Fig. 2(a) with unit cell parameters of $a_h = 5.440(2)$ Å and $c_h = 13.124(5)$ Å. However, the patterns for the sintered samples with $0.5 \leqslant x \leqslant 0.75$ are indexed in a cubic system, similarly to what is observed in $SrCoO_3$ compound ($Pm\bar{3}m$ space group, PDF Card No. 38-1148 [23], Fig. 2(b)). The unit cell parameter is $a = 3.833(2)$ Å for the $La_{0.25}Ba_{0.75}CoO_3$ sample. These results are consistent with those of Luo and Wang [33]. Indeed, they have detected a structural phase transformation from $R\bar{3}c$ to $Pm\bar{3}m$ at $x = 0.30$–0.35. Finally, as the Ba content increases, peak positions shift to lower 2θ values which are consistent with the substitution of lanthanum cations by larger barium cations, 1.36 and 1.61 Å, respectively [34].

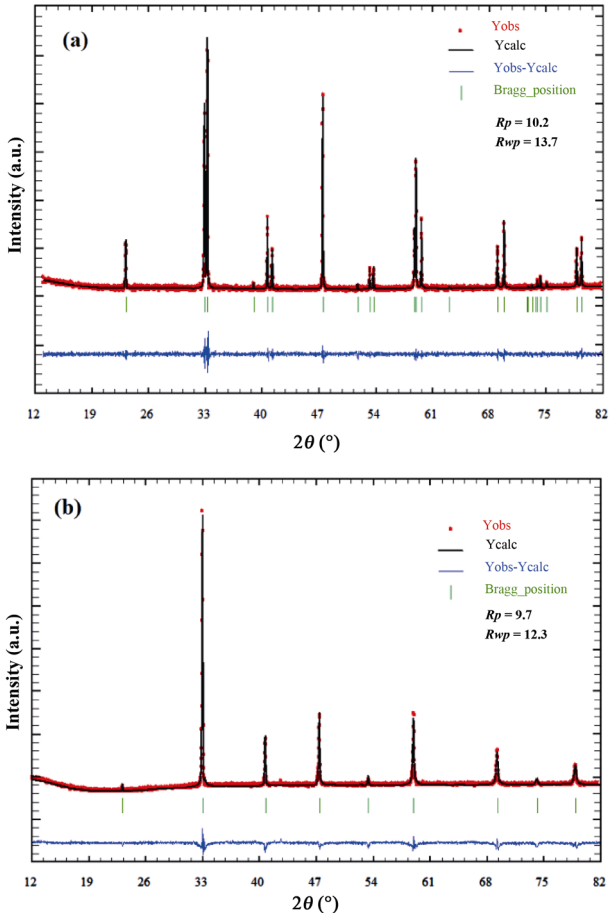

Fig. 2 Rietveld refinement results of XRD patterns for (a) $La_{0.9}Ba_{0.1}CoO_3$ ($x = 0.1$) and (b) $La_{0.25}Ba_{0.75}CoO_3$ ($x = 0.75$). The experimental data are shown as dots; the global fitting profile and the difference curve are shown as solid lines; the calculated reflection positions are indicated by stick marks.

Figure 3 shows the microstructure of $La_{1-x}Ba_xCoO_3$ pellets examined by FEG-SEM. For $x < 0.5$, it is noted that with increasing Ba content, an increase in grain size is observed. The grain size of these samples is in the range of 20–50 μm. All these samples are dense sintered ceramics, indicating the effectiveness of conventional sintering in preparing such ceramics. These ceramics have high relative densities in the range of 94%–98%.

For $x \geqslant 0.5$, after the rhombohedral–cubic transition, the samples showed high compactness ($\leqslant$ 92%). However, a remarkable decrease in grain size was noted ($\leqslant$ 15 μm).

Figure 4(a) exhibits the Ba substitution content dependence (x) of the electrical conductivity (σ) of the $La_{1-x}Ba_xCoO_3$ sample at 330 K. The electrical conductivity σ presents an optimum value for $x = 0.25$ with a value of $\sigma_{max} \approx 2.2\times10^5$ S·m^{-1}. Indeed, measurements of the electrical conductivity show that the ceramics substituted by Ba display a high electric conductivity at low temperatures. This value is slightly lower than the optimum electrical conductivity in $La_{1-x}Sr_xCoO_3$, which is $\sigma_{max} \approx 3\times10^5$ S·m^{-1} at 330 K for $x = 0.3$ [23]. However, it is consistent in terms of substitutant content. This is also consistent with Khalil's data [30] that reported the highest electrical conductivities between room temperature and 573 K for $x = 0.3$ in $La_{1-x}Ba_xCoO_3$ samples prepared by sol-gel. For $x > 0.25$, σ decreases with increasing Ba concentration.

The temperature dependence of σ of the $La_{1-x}Ba_xCoO_3$ sample with $x = 0.05$ from 330 to 1000 K is shown in Fig. 4(b). At lower temperatures, the electrical conductivity increases when temperature increases which is the characteristic of a semiconducting behaviour. Then, σ starts decreasing upon higher temperatures, exhibiting an insulator–metal (I–M) transition around 800 K. This behaviour is attributed to closing of charge-transfer gap caused by the expansion of Co-3d and O-2p bandwidths regardless of the spin state of Co^{3+} [35,36]. Similar variation in electrical conductivity as a function of temperature was observed in previous study [37]. Indeed, they found that the $La_{1-x}Ba_xCoO_3$ samples become metallic at temperatures above 700 K.

At 330 K, S of the $La_{1-x}Ba_xCoO_3$ sample is plotted as a function of the Ba concentration (x) (Fig. 5(a)). The Seebeck coefficient of the $La_{1-x}Ba_xCoO_3$ sample for $x = 0$ shows a negative value (–250 μV·K^{-1}), while, it becomes positive for $x > 0$. Then, it can be deduced that the substitution of La^{3+} by Ba^{2+}, even at low levels, leads to a change of carrier type. The highest value

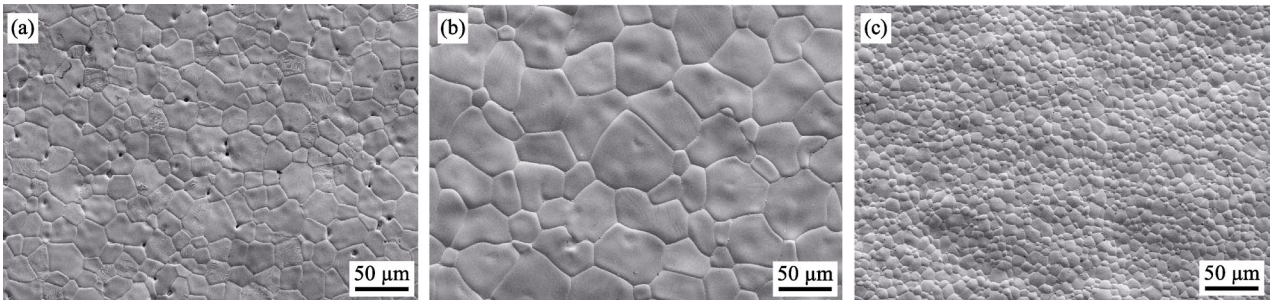

Fig. 3 SEM micrographs of (a) $La_{0.95}Ba_{0.05}CoO_3$, (b) $La_{0.9}Ba_{0.1}CoO_3$, and (c) $La_{0.25}Ba_{0.75}CoO_3$.

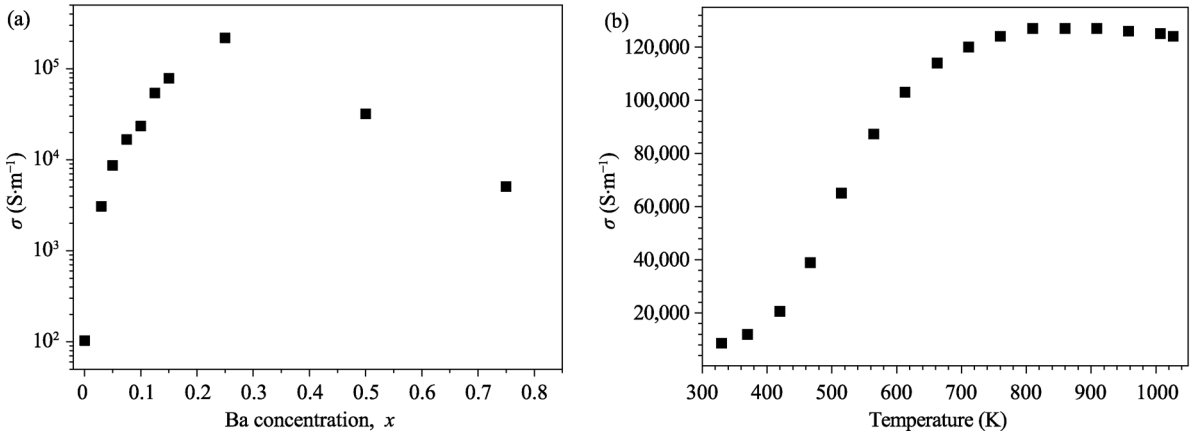

Fig. 4 σ for $La_{1-x}Ba_xCoO_3$ (a) with $0 \leqslant x \leqslant 0.75$ at 330 K and (b) with $x = 0.05$ at different temperatures.

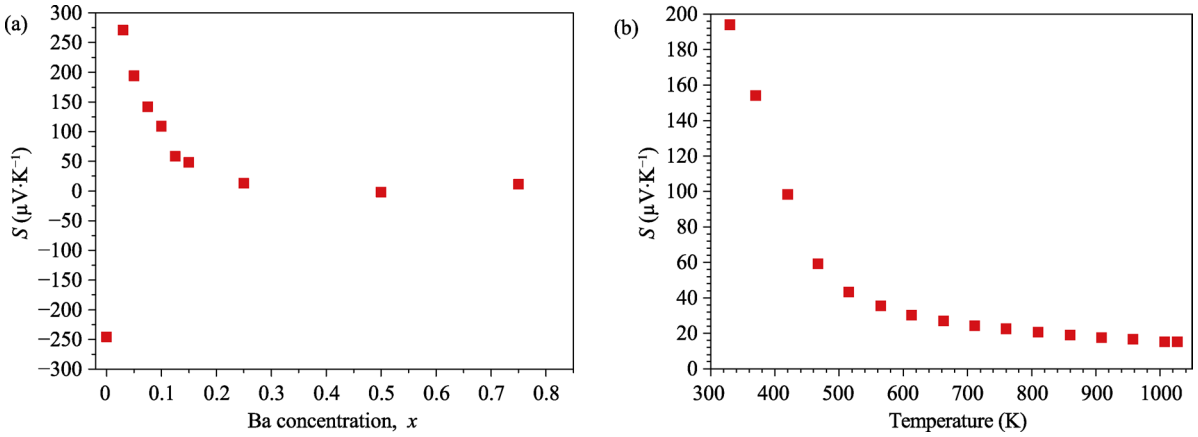

Fig. 5 S for $La_{1-x}Ba_xCoO_3$ (a) with $0 \leqslant x \leqslant 0.75$ at 330 K and (b) with $x = 0.05$ at different temperatures.

(S = 271 μV·K^{-1}) is observed for $x = 0.03$. Kun *et al.* [37] found that, for the same Ba content, S exhibits a value close to our value, whereas for lower Ba content (1%), a higher value of S (≈ 400 μV·K^{-1}) was measured. This is similar to the values measured in $La_{1-x}Sr_xCoO_3$ compounds but for higher substitutant content ($x = 0.05$) [23].

For $x > 0.03$, S decreases with increasing Ba concentration. The decrease of S with increasing x shows that the carrier concentration increases as a function of x. This is consistent with the substitution of trivalent La^{3+} cations by divalent Ba^{2+} cations and the increase of electrical conductivity. Furthermore, we notice that for values of $x > 0.15$, S presents very low value, which indicates the high electrical conductivity of samples. This decrease in S values is expected because additional charge carriers are introduced when the Ba^{2+} substitution rate increases.

Figure 5(b) depicts the temperature dependence of S of the $La_{1-x}Ba_xCoO_3$ sample with $x = 0.05$ from 330 to 1000 K. S of the $La_{1-x}Ba_xCoO_3$ sample shows a positive value over the whole measured temperature range, indicating p-type conduction. However, the value of S roughly decreases with increasing temperature. From 330 to 500 K, the value of S strongly decreases from 194 to 42 μV·K^{-1}. Then, in the range of 500–1000 K, it decreases softly to reach 15 μV·K^{-1}.

By combining S and electrical conductivity, the dependence of PF as a function of the Ba concentration for these samples is shown in Fig. 6. The value of PF increases when Ba concentration tends to the value of 0.075. The best PF value reaches 3.4×10^{-4} W·m^{-1}·K^{-2} at 330 K for $x = 0.075$. This value is three times higher than the one reported by Kun *et al.* [37] ($x = 0.05$ at 350 K) due to their low density and therefore low

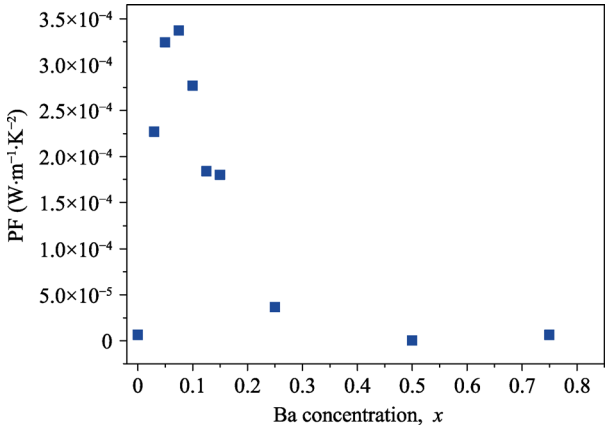

Fig. 6 PF for $La_{1-x}Ba_xCoO_3$ with $0 \leqslant x \leqslant 0.75$ at 330 K.

electrical conductivity.

For $0.075 \leqslant x \leqslant 0.75$, the value of PF roughly decreases to reach a value of almost zero for $x \geqslant 0.5$. It is important to note that the optimum PF value is 10% higher than the one obtained in $La_{1-x}Sr_xCoO_3$ compounds [23] and that is obtained for $x = 0.075$ and 0.05, respectively, whereas both strontium and barium are divalent cations. This clearly emphasizes the influence of other parameters (such as orbital recovery due to changes in the morphology or tilting of octahedra) than the only charge carriers concentration in the transport properties of La or Sr-substituted $LaCoO_3$ ceramics.

Temperature dependence of κ of the $La_{1-x}Ba_xCoO_3$ sample with $0 \leqslant x \leqslant 0.1$ from 330 to 1000 K is shown in Fig. 7. It is noted that, for all compositions, as the temperature increases, κ increases to reach a maximum value of 7.53 W·m^{-1}·K^{-1} for $x = 0.1$ at 1000 K. Moreover, whatever the temperature, κ increases when the substitution rate increases. Indeed, this increase in κ can be correlated with the increase in

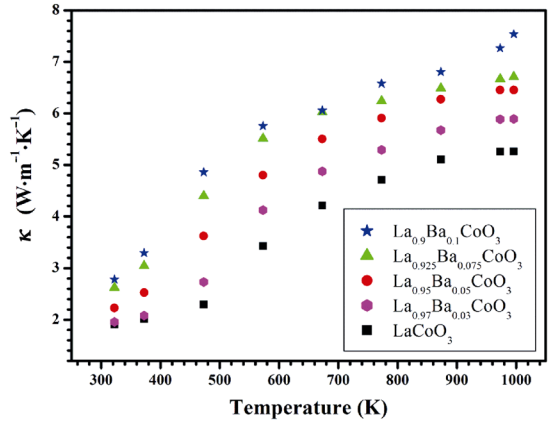

Fig. 7 Temperature dependence of κ of the $La_{1-x}Ba_xCoO_3$ sample with x = 0, 0.03, 0.05, 0.075, and 0.1.

electrical conductivity that increases when temperature or Ba content increases. κ of $La_{1-x}Ba_xCoO_3$ sample with x = 0.05 is lower than for the sample with the same Sr content probably due to the heavier character of barium compared to strontium. However, when the optimum PF values are at 330 K (x = 0.05 and 0.075 for Sr and Ba, respectively), thermal conductivities are pretty similar.

Figure 8 shows the temperature dependence of ZT of the $La_{1-x}Ba_xCoO_3$ sample with $0 \leqslant x \leqslant 0.1$ from 330 to 1000 K. ZT shows a maximum value of 0.048 for x = 0.05 at 330 K. It rapidly decreases when the temperature increases. Decrease in ZT as a function of temperature is attributed to both the decrease in S and increase in κ. Compared to $La_{1-x}Sr_xCoO_3$ compounds that present the highest ZT of 0.038 for x = 0.05, two values in Ba-substituted samples are higher, for x = 0.075 (the best PF) and x = 0.05. On the contrary

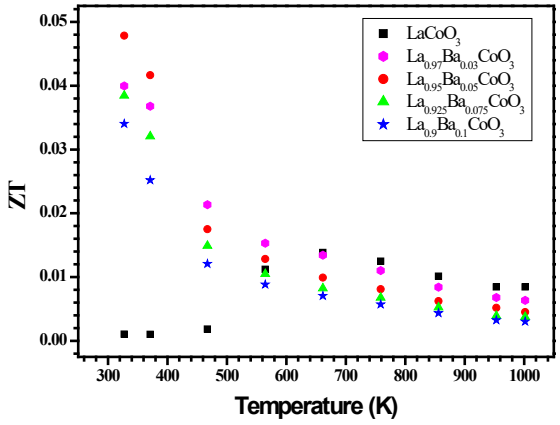

Fig. 8 Temperature dependence of the ZT value of the $La_{1-x}Ba_xCoO_3$ sample with x = 0, 0.03, 0.05, 0.075, and 0.1.

to $La_{1-x}Sr_xCoO_3$ compounds, the sample with the best ZT value is not the one with the highest PF. The ZT value for x = 0.05 is similar to the one reported by Kun *et al*. [37] for the same Ba content, even if the sample made from particles synthesized by sol-gel method is porous.

4 Conclusions

The $La_{1-x}Ba_xCoO_3$ samples ($0 \leqslant x \leqslant 0.75$) have been synthesized by solid state reaction and conventionally sintered. Their structural and thermoelectric properties have been studied in the range of 330–1000 K. After several thermal cycles, pure and dense ceramics are obtained over the whole composition range. XRD characterization shows a structural change from rhombohedral to cubic perovskite phase for $x \geqslant 0.5$. For $x > 0.75$, even with the addition of silicon, samples do not present a cubic perovskite.

Electrical and thermal properties exhibit strong variations when x varies: the electrical conductivity exhibits an optimum value for x = 0.25 ($\sigma_{max} \approx 2.2\times10^5$ S·m^{-1}), while S decreases when x and/or temperature increases. The $La_{1-x}Ba_xCoO_3$ presents a p-type semiconducting behaviour. The value of PF increases to reach 3.4×10^{-4} W·m^{-1}·K^{-2} at 330 K when x = 0.075. This value is 10% higher than the best one obtained in $La_{1-x}Sr_xCoO_3$ compounds. The lowest κ is observed at low temperatures for small x values. Finally, the best thermoelectric properties are observed at low temperatures: the highest ZT value of 0.048 is achieved at 330 K for x = 0.05. It is 25% higher than the best ZT value in $La_{1-x}Sr_xCoO_3$ compounds.

Acknowledgements

The authors acknowledge Programme d'Investissment d'Avenir PIA "Tours 2015" for the financial support.

References

[1] Radaelli PG, Cheong SW. Structural phenomena associated with the spin-state transition $InLaCoO_3$. *Phys Rev B* 2002, **66**: 094408.

[2] Maris G, Ren Y, Volotchaev V, *et al*. Evidence for orbital ordering $InLaCoO_3$. *Phys Rev B* 2003, **67**: 224423.

[3] Knížek K, Jirák Z, Hejtmánek J, *et al*. Structural anomalies associated with the electronic and spin transitions in $LnCoO_3$. *Eur Phys J B* 2005, **47**: 213–220.

[4] Zobel C, Kriener M, Bruns D, *et al*. Evidence for a low-spin to intermediate-spin state transition $InLaCoO_3$. *Phys Rev B* 2002, **66**: 020402.

[5] Sazonov AP, Troyanchuk IO, Gamari-Seale H, *et al*. Neutron diffraction study and magnetic properties of $La_{1-x}Ba_xCoO_3$ (x = 0.2 and 0.3). *J Phys: Condens Matter* 2009, **21**: 156004.

[6] Terasaki I, Sasago Y, Uchinokura K. Large thermoelectric power in $NaCo_2O_4$ single crystals. *Phys Rev B* 1997, **56**: R12685–R12687.

[7] Li SW, Funahashi R, Matsubara I, *et al*. High temperature thermoelectric properties of oxide $Ca_9Co_{12}O_{28}$. *J Mater Chem* 1999, **9**: 1659–1660.

[8] Masset AC, Michel C, Maignan A, *et al*. Misfit-layered cobaltite with an anisotropic giant magnetoresistance: $Ca_3Co_4O_9$. *Phys Rev B* 2000, **62**: 166–175.

[9] Delorme F, Martin CF, Marudhachalam P, *et al*. Effect of Ca substitution by Sr on the thermoelectric properties of $Ca_3Co_4O_9$ ceramics. *J Alloys Compd* 2011, **509**: 2311–2315.

[10] Saini S, Yaddanapudi HS, Tian K, *et al*. Terbium ion doping in $Ca_3Co_4O_9$: A step towards high-performance thermoelectric materials. *Sci Rep* 2017, **7**: 44621.

[11] Delorme F, Diaz-Chao P, Giovannelli F. Effect of Ca substitution by Fe on the thermoelectric properties of $Ca_3Co_4O_9$ ceramics. *J Electroceram* 2018, **40**: 107–114.

[12] Yamauchi H, Sakai K, Nagai T, *et al*. Parent of misfit-layered cobalt oxides: $[Sr2O_2]_qCoO_2$. *Chem Mater* 2006, **18**: 155–158.

[13] Funahashi R, Shikano M. $Bi_2Sr_2Co_2O_y$ whiskers with high thermoelectric figure of merit. *Appl Phys Lett* 2002, **81**: 1459–1461.

[14] Diez JC, Guilmeau E, Madre MA, *et al*. Improvement of $Bi_2Sr_2Co_{1.8}O_x$ thermoelectric properties by laser floating zone texturing. *Solid State Ionics* 2009, **180**: 827–830.

[15] Madre MA, Costa FM, Ferreira NM, *et al*. High thermoelectric performance in $Bi_{2-x}Pb_xBa_2Co_2O_y$ promoted by directional growth and annealing. *J Eur Ceram Soc* 2016, **36**: 67–74.

[16] Funahashi R, Barbier T. Thermoelectric properties of $(BaCoO_{3-y})_nBaCo_8O_{11}$. *AIP Conf Proc* 2016, **1763**: 030004.

[17] Delorme F, Chen C, Pignon B, *et al*. Promising high temperature thermoelectric properties of dense $Ba_2Co_9O_{14}$ ceramics. *J Eur Ceram Soc* 2017, **37**: 2615–2620.

[18] Cong C, Delorme F, Schoenstein F, *et al*. Synthesis, sintering, and thermoelectric properties of $Co_{1-x}M_xO$(M = Na, $0 \leqslant x \leqslant 0.07$; M = Ag, $0 \leqslant x \leqslant 0.05$). *J Eur Ceram Soc* 2019, **39**: 346–351.

[19] Androulakis J, Migiakis P, Giapintzakis J. $La_{0.95}Sr_{0.05}CoO_3$: An efficient room-temperature thermoelectric oxide. *Appl Phys Lett* 2004, **84**: 1099–1101.

[20] Zhang X, Li XM, Tong LC, *et al*. Thermoelectric and transport properties of $La_{0.95}Sr_{0.05}CoO_3$. *J Cryst Growth* 2006, **286**: 1–5.

[21] Kozuka H, Yamada H, Hishida T, *et al*. Electronic transport properties of the perovskite-type oxides $La_{1-x}Sr_xCoO_{3\pm\delta}$. *J Mater Chem* 2012, **22**: 20217–20222.

[22] Papageorgiou C, Athanasopoulos GI, Kyratsi T, *et al*. Influence of processing conditions on the thermoelectric properties of $La_{1-x}Sr_xCoO_3$(x=0, 0.05). *AIP Conf Proc* 2012, **1449**: 323–326.

[23] Bousnina MA, Dujardin R, Perriere L, *et al*. Synthesis, sintering, and thermoelectric properties of the solid solution $La_{1-x}Sr_xCoO_{3\pm\delta}$ ($0 \leqslant x \leqslant 1$). *J Adv Ceram* 2018, **7**: 160–168.

[24] Muta K, Kobayashi Y, Asai K. Magnetic, electronic transport, and calorimetric investigations of $La_{1-x}Ca_xCoO_3$ in comparison with $La_{1-x}Sr_xCoO_3$. *J Phys Soc Jpn* 2002, **71**: 2784–2791.

[25] Masuda H, Fujita T, Miyashita T, *et al*. Transport and magnetic properties of $R_{1-x}A_xCoO_3$(R = La, Pr and Nd; A = Ba, Sr and Ca). *J Phys Soc Jpn* 2003, **72**: 873–878.

[26] Kozuka H, Yamagiwa K, Ohbayashi K, *et al*. Origin of high electrical conductivity in alkaline-earth doped $LaCoO_3$. *J Mater Chem* 2012, **22**: 11003–11005.

[27] Sánchez RD, Mira J, Rivas J, *et al*. Magnetoresistance, temporal evolution, and relaxation of the electrical resistivity in the re-entrant semiconducting $La_{0.80}Ba_{0.20}CoO_3$ perovskite. *J Mater Res* 1999, **14**: 2533–2539.

[28] Barman A, Ghosh M, De SK, *et al.* Electrical transport properties of bulk $La_{1-x}Ba_xCoO_3$ at low temperature. *Phys Lett* 1997, **234**: 384–390.

[29] Patil SB, Keer HV, Chakrabarty DK. Structural, electrical, and magnetic properties in the system $Ba_xLa_{1-x}CoO_3$. *Phys Stat Sol* (*a*) 1979, **52**: 681–686.

[30] Khalil MS. Synthesis, X-ray, infrared spectra and electrical conductivity of La/Ba–CoO_3 systems. *Mater Sci Eng* 2003, **352**: 64–70.

[31] Rodríguez-Carvajal J. Recent advances in magnetic structure determination by neutron powder diffraction. *Phys B Condens Matter* 1993, **192**: 55–69.

[32] Closset NMLNP, Van Doorn RHE, Kruidhof H, *et al*. About the crystal structure of $La_{1-x}Sr_xCoO_{3-\delta}$ ($0 \leqslant x \leqslant 0.6$). *Powder Diffr* 1996, **11**: 31–34.

[33] Luo WJ, Wang FW. Powder X-ray diffraction and Rietveld analysis of $La_{1-x}Ba_xCoO_3$ ($0 < x \leqslant 0.5$). *Powder Diffr* 2006, **21**: 304–306.

[34] Shannon RD. Revised effective ionic radii and systematic studies of interatomic distances in halides and chalcogenides. *Acta Cryst Sect A* 1976, **32**: 751–767.

[35] Cong C, Giovannelli F, Chartier T, *et al*. Synthesis and thermoelectric properties of doubly substituted $La_{0.95}Sr_{0.05}Co_{1-x}Cr_xO_3$ ($0 \leqslant x \leqslant 0.5$). *Mater Res Bull* 2018, **102**: 257–261.

[36] Iwasaki K, Ito T, Nagasaki T, *et al*. Thermoelectric properties of polycrystalline $La_{1-x}Sr_x$ CoO_3. *J Solid State Chem* 2008, **181**: 3145–3150.

[37] Kun R, Populoh S, Karvonen L, *et al*. Structural and thermoelectric characterization of Ba substituted $LaCoO_3$

perovskite-type materials obtained by polymerized gel combustion method. *J Alloys Compd* 2013, **579**: 147–155.